Chinese Chemical Letters 33 (2022) 3303–3314

Contents lists available at ScienceDirect

Chinese Chemical Letters

journal homepage: www.elsevier.com/locate/cclet

Stable isotope labeling of nanomaterials for biosafety evaluation and drug development

Xue-Ling Chang[a,*], Lingyun Chen[a], Boning Liu[a], Sheng-Tao Yang[b,*], Haifang Wang[c], Aoneng Cao[c], Chunying Chen[d,*]

[a] CAS Key Laboratory for Biomedical Effects of Nanomaterials and Nanosafety, Institute of High Energy Physics, Chinese Academy of Sciences, Beijing 100049, China
[b] Key Laboratory of Pollution Control Chemistry and Environmental Functional Materials for Qinghai-Tibet Plateau of the National Ethnic Affairs Commission, School of Chemistry and Environment, Southwest Minzu University, Chengdu 610041, China
[c] Institute of Nanochemistry and Nanobiology, Shanghai University, Shanghai 200444, China
[d] CAS Key Laboratory for Biomedical Effects of Nanomaterials and Nanosafety and CAS Center for Excellence in Nanoscience, National Center for Nanoscience and Technology of China, and University of Chinese Academy of Sciences, Beijing 100190, China

ARTICLE INFO

Article history:
Received 18 February 2022
Revised 13 March 2022
Accepted 14 March 2022
Available online 18 March 2022

Keywords:
Stable isotope labeling
Quantification
Carbon nanomaterials
Metal oxide nanoparticles
Nanotoxicity
Biomedical effects

ABSTRACT

Quantitative information, such as environmental migration, absorption, biodistribution, biotransformation, and elimination, is fundamental and essential for the nanosafety evaluations of nanomaterials. Due to the complexity of biological and environmental systems, it is challenging to develop quantitative approaches and tools that could characterize intrinsic behaviors of nanomaterials in the organisms. The isotopic tracers are ideal candidates to tune the physical properties of nanomaterials while preserving their chemical properties. In this review article, we summarized the stable isotope labeling methods of nanomaterials for evaluating their environmental and biological effects. The skeleton labeling protocols of carbon nanomaterials and metal/metal oxide nanoparticles were introduced. The advantages and disadvantages of stable isotope labeling were discussed in comparison with other quantitative methods for nanomaterials. The quantitative information of nanomaterials in environmental and biological systems was summarized along with the biosafety data. The benefits for drug development of nanomedicine were analyzed based on the targeting effects, persistent accumulation, and safety. Finally, the challenges and future perspectives of stable isotope labeling in nanoscience and nanotechnology were discussed.

1. Introduction

With the rapid development and wide applications of nanotechnology, thousands of nano products are entering our daily life and the environment. Among them, carbon, metal and metal oxide nanomaterials are the typical examples of the most used commercial nanomaterials because of their unique physicochemical properties and high performance [1–3]. In the process of production, use and treatment, nanomaterials will inevitably enter the environment, just like the two sides of a coin, which may have positive and/or negative impacts on the ecological environment through the biosphere and through the trophic transfer of ecosystem food chains [4–10]. Particularly, the biological effects and safety of nanomaterials are important properties for the future development and applications of nanomaterials in industry, agriculture, medicine and other fields. They have become key components underpinning the environmental and health risk assessment of nanomaterials. The environmental health effects of nanomaterials have attracted great attention from the scientific community and governments worldwide [11–15]. The public focus and concern regarding the biological effects and safety of nanomaterials started more than 20 years ago. The United States, the United Kingdom, the European Union and many other developed countries have successively formulated long-term strategic plans in the field of nanosafety assessment, and the research projects and funding increase rapidly. As early as 2002, the Chinese Academy of Sciences (CAS) established the Key Laboratory of Biomedical Effects and Nanosafety of the Chinese Academy of Sciences in Beijing. It is the first institution that focuses on the research of biomedical effects and nanosafety in China. The laboratory has studied the absorption, distribution, metabolism, excretion, and toxicity (ADME/T) of nanomaterials from different levels, such as molecule-cell-tissue-whole

* Corresponding authors.
E-mail addresses: changxl@ihep.ac.cn (X.-L. Chang), yangst@swun.edu.cn (S.-T. Yang), chenchy@nanoctr.cn (C. Chen).

https://doi.org/10.1016/j.cclet.2022.03.057
1001-8417/

animal, and achieved a series of internationally influential achievements [16–32]. In 2006, the Chinese government launched the 973 program "Nanotoxicological study of manufactured nanomaterials: China nanosafety research project", supporting the research on the unique physical and chemical properties of nanomaterials, the characteristics and laws of interaction with organisms and its mechanism, and the nanosafey research obtained continuous research support and funding. Currently, there are some reports on the environmental biological effects and toxicity of nanomaterials, such as fullerene C_{60}, carbon nanotubes (CNTs), ZnO, TiO_2, CeO_2, Ag and quantum dots (QDs), which are toxic to diverse organisms (*e.g.*, rat, mouse, fish, *Daphnia magna*, algae and plants) [27,33–52]. According to the environmental safety data of nanomaterials, the US Environmental Protection Agency has listed nanomaterials as emerging environmental pollutants. Obviously, the biomedical effects and potential hazards of nanomaterials have been widely recognized by the scientific community. A nanomaterial's biological effects and nanosafety profile have become important prerequisites for the applications of nanomaterials. The nanosafety study has become an indispensable part of the basic research framework of nanoscience and nanotechnology.

For the environmental biological effects and safety of nanomaterials, there is an urgent need to clearly understand whether the physicochemical properties and bio-effects of nanomaterials change with the influence of environmental conditions after entering the environment [10,20,53–55]. Of particular, the information on the migration, absorption, biodistribution, biotransformation and elimination of nanomaterials should be thoroughly obtained in the actual environment and biological systems. Due to the limitations of existing research methods for intrinsic properties of nanomaterials (especially carbon nanomaterials, which have high biological background of carbon atoms), the role and interaction law of nanomaterials at different levels and between each other in organisms and the environmental systems are largely unknown. Even for the same nanomaterials, such as CNTs, QDs, or TiO_2 nanoparticles (NPs), although there are numerous biological effect studies, their toxicity results are often controversial [9,13,37–39]. The studies of bioaccumulation, nutrient transfer and biomagnification of nanomaterials at different trophic levels of food chain are also challenging due to the extremely low concentrations in samples. To investigate the biological behaviors of nanomaterials in complex biological and environmental systems, the accurate detection methods must be firstly developed and established, especially for carbon nanomaterials and trace metal/metal oxide nanomaterials [18,21,23,56]. The quantification technologies have become the key basis for the environmental safety assessments of nanomaterials.

Taking carbon nanomaterials as an example, the physicochemical properties of carbon nanomaterials, including their size, shape, aspect ratio, charge, composition and surface chemistry, together with exposure route and dose, have significant impacts on their ADME/T in living organisms and food chain, thereby affecting their applications in biomedicine, food, agriculture and so on [50–52]. However, the high carbon background in the environmental/biological system and the much lower concentration of carbon nanomaterials make the quantification of *in vivo* uptakes of carbon nanomaterials very difficult [25,26]. Some methods have been applied to analyze the unmodified carbon nanomaterials, such as high-performance liquid chromatography (HPLC) coupled with mass spectrometry (MS), electron microscope, Raman spectroscopy and radioactive isotopic labeling [57–65], but these methods suffer disadvantages of limited application range, low sensitivity, or radioactive pollution [61–63]. Alternatively, stable isotope ^{13}C skeleton-labeling is a simple but powerful technique with high sensitivity and specificity, which is the preferred choice to quantify carbon nanomaterials *in vivo* [23,25,26]. Prof. Zhifang Chai from the Institute of High Energy Physics and Yuanfang Liu from Peking University initiated the isotope labeling methods with carbon nanotubes as earlier in 2003 with the support by the major project of National Natural Science Foundation of China [25,66].

In this article, we critically reviewed a new category of analytical methods based on stable isotopic labeling technology for the isotopic effect of structure, biomedical effects and nanosafety studies of carbon nanomaterials and metal/metal oxide nanoparticles. The applications of ^{13}C-skeleton labeled fullerene, CNTs, graphene, graphdiyne, and ^{13}C enrichment in carbon NPs and carbon QDs (CQDs), as well as some metal stable isotope labeled NPs using $^{107}Ag/^{109}Ag$, $^{68}Zn/^{67}Zn/^{70}Zn$, $^{142}Ce/^{140}Ce$, ^{47}Ti, ^{57}Fe and ^{65}Cu in diverse models along with the detecting methods of isotope-enriched samples were listed in Table 1 [42–49,56,58,67–109]. Bioaccumulation, biodistribution, transformation, metabolism, elimination and toxicity of these nanomaterials in animals and plants were evaluated quantitatively through the stable isotope labeling methods. Nutrient transfer and biomagnification of nanomaterials at terrestrial/aquatic food chains were traced for long-term. The potential benefits of stable isotope labeling methods for the development of nanomedicine were analyzed.

2. Characteristics of stable isotope labeling

2.1. Characteristics of ^{13}C-labeling

Traditional approaches for quantitatively estimating the biological behaviors and structure of small molecule chemicals, such as chromatography, mass spectrometry, and nuclear magnetism, have been shown to be unsuitable for the quantitative analysis of nanomaterials in environmental and organisms, and it is a challenge to establish a safe and non-destructive quantitative analysis method for nanomaterials. At present, the most widely used quantitative analysis methods for carbon nanomaterial are fluorescent labeling and radioactive labeling [18,25,110,111]. Fluorescent labeling is very vulnerable in complicated systems and not suitable for long-term evaluations. The fluorescent labeling is through chemical functionalization, except for intrinsic fluorescent CQDs [67,68,81]. Thus, the fluorescent labeling inevitably changes the properties of carbon nanomaterials. On the other hand, many radioactive isotopes, such as ^{14}C, ^{67}Ga, ^{99m}Tc, ^{125}I and ^{166}Ho, were used to label carbon nanomaterials to study their quantitative biodistribution in animals [112–122]. However, it is obvious that the radioactive labeling suffers several drawbacks. In general, the conditions for radioactive labeling and the subsequent operation are not available for most toxicologists and pharmacologists, and the radioactive waste is seriously concerned. Further, except ^{14}C, the rest isotopes could only be applied in studying the functionalized carbon nanomaterials. As an alternative, the long-lived radioactive isotope ^{14}C ($t_{1/2} = 5730$ y), which is appropriate for the long-term tracing studies, has been often used for labeling fullerene. However, the whole procedure of synthesis, detection and waste treatment of ^{14}C-carbon nanomaterials is quite difficult.

Given the disadvantages of fluorescent labeling and radioactive labeling, the stable isotope labeling is a good choice. It avoids radioactive operation and wastes. Generally, a stale isotope of the element of interest is incorporated into the molecule or product, then, any related transformations can be easily and precisely detected according to the relative abundance of stable isotopes by inductively coupled mass spectrometry (ICP-MS), high resolution ICP-MS, multi-collector ICP-MS (MC-ICP-MS), or thermal ionization MS (TIMS) and isotope ratio mass spectrometry (IRMS) [111,123–128]. For carbon nanomaterials, carbon isotope ratios are measured relative to the internationally recognized C standard Vienna Pee Dee Belemnite (VPDB) and are reported in the delta notation [42,129]. The ^{13}C-labeling is an ideal choice for the quantification of car-

Table 1
Representative stable isotopes for labeling nanomaterials.

Stable isotopes	Nanomaterials	Models	Detectors	Refs.
^{13}C	fullerene, CNTs, graphene, graphdiyne, carbon NPs, CQDs	mouse, *S. obliquus*, *D. magna*, *D. rerio*, white rot basidiomycete fungi, soil microorganisms, marine mussel, wheat, pea, macrophage	IRMS, MR	[42–49,58,67–87]
$^{107}Ag/^{109}Ag$	Ag NPs	sediment, water, *L. stagnalis*, *A. thaliana*, rice	quadruple ICP-MS, MC-ICP-MS, single particle ICP-MS, NanoSIMS	[56,88–94]
^{68}Zn	ZnO NPs	earthworm, soil, pore water, *P. australis*, skin of human, mice, HaCaT cell	MC-ICP-MS, ICP-OES, TOF-SIMS	[95–99]
^{67}Zn	ZnO NPs	*S. plana*, *N. diversicolor*	ICP-MS, ICP-OES	[100,101]
^{70}Zn	ZnO NPs	*A. thaliana*	ICP-MS, ICP-OES	[92,101]
$^{142}Ce/^{140}Ce$	CeO_2 NPs	soil, CeO_2 materials, Ce	MC-ICP-MS, ICP-TOFMS, TIMS	[102–104]
^{47}Ti	TiO_2 NPs	Mussel	ICP-MS	[56,105]
^{57}Fe	goethite nanorods, $Fe@SiO_2$ NPs	water, natural iron colloid grade	MC-ICP-MS, Sector field ICP-MS	[106,107]
^{65}Cu	CuO NPs, Cu NPs	*L. stagnalis*, *A. thaliana*	ICP-OES, ICP-MS	[92,108,109]

Table 2
Characteristics of ^{13}C-labeling comparing with radioactive labeling methods.

	Detection sensitivity	Labeling stability	Labeling protocol	Sampling	Imaging capability	Waste handling
^{13}C	High	High	Moderate	Homogenization	Poor	None
^{14}C	Ultrahigh	High	Difficult/moderate	Digestion	Moderate	Radioactive wastes
^{3}H	Ultrahigh	Moderate	Moderate	Digestion	Moderate	Radioactive wastes
Radioactive metals	Ultrahigh	Moderate	Facile/moderate	None	High	Radioactive wastes

bon nanomaterials. Stable isotopes represent a degree of freedom that might be exploited to tune the physical properties of materials while preserving their chemical behaviors [69,130–141]. The specific advantages and complements include: First, the unfavorable factors of radiolabeling can be avoided; Second, stable isotope ^{13}C replaces the skeleton carbon atoms of labeled carbon nanomaterials, which does not introduce exogenous atoms, and the intrinsic properties are retained; Third, the skeleton-labeled carbon nanomaterials have the same stability of original ones, thus suitable for long-term tracing; Fourth, the increase of the $^{13}C/^{12}C$ signal in the IRMS test is large by ^{13}C-labeling, so the sensitivity of the detection is greatly improved, reaching trace analysis (ppt); Fifth, this skeleton labeling enhances the Raman and nuclear magnetic signals of carbon nanomaterials, providing the possibility of developing new analytical methods. In a word, the stable isotopic labeling technology, as one of advanced nuclear analytical techniques, has the advantages of satisfied sensitivity, accurate positioning, nondestructive, quantitative analysis, and convenient operation.

The main drawback of ^{13}C-labeling comparing to radiolabeling is the lower sensitivity, due to the interference of natural ^{13}C background (1.1%). Comparing with fluorescent labeling, the visualization of ^{13}C-labeled carbon nanomaterials is more difficult, because of the low spatial resolutions, despite the recent achievements by laser ablation-isotope ratio mass spectrometry (LA-IRMS) [82,142]. The merits and drawbacks of stable isotope labeling methods are compared in Table 2.

2.2. Characteristics of stable metal isotope labeling

Isotopes are atoms of an element with different numbers of neutrons and thus different masses. They behave very similarly in most chemical reactions, which are governed by the nuclear charge, defined by the number of protons, and the configuration of the outer electron shells. Most elements in the periodic table consist of mixtures of multiple stable isotopes, with their weighted average determining the atomic mass. For instance, copper consists of two stable isotopes (^{63}Cu, ^{65}Cu) with relative abundances of 69.2% and 30.8%, respectively, resulting in an atomic mass of 63.546 g/mol. Some elements consist of mixtures of two or more stable isotopes (up to 10) which potentially allows deducing the information about their environmental cycling from stable isotope variations. Stable metal isotope labeling technique is able to change the isotopic abundance in metal/metal oxide nanoparticles. The variations in isotopic abundance of environment and/or organism samples were determined with inductively coupled plasma mass spectrometry (ICP-MS). Generally, tracing metal-based engineering NPs (MENPs) with highly enriched isotopes of low natural abundance provides the best sensitivity, so as to achieve the high detection sensitivity of the isotope-labeled MENPs [127]. While, due to the difficulty of preparation and enrichment, enriched isotopes with a low natural abundance are typically more expensive than those with a high natural abundance, which increases the cost of labeling. In addition, the choice of enriched isotope is strongly constrained by potential interference occurring in the sample or the measurement procedure. The main disadvantage in the preparation of MENPs labeled with stable isotopes is that the universal and easily accessible MENPs cannot be effectively labeled with stable isotopes post-synthesis. This is a technical challenge mainly regarding the inability to obtain raw materials enriched in natural abundance stable isotope, and the low yield and high cost of the material synthesis process.

However, with the developments in inorganic mass spectrometric instrumentation including ICP-MS and MC-ICP-MS for determining the variations and concentrations of metal stable isotope in complex matrix, which presents high sensitivity, wide dynamic linear range, and more importantly multiplex and absolute quantification ability in distinguishing from the endogenous background metal in various samples [123–128]. Metal stable isotope labeling has some unique advantages, such as, the metal stable isotope tags do not need to possess radioactive, optical, electric, electro-

chemical, magnetic, or any other special properties, since isotope atoms inside the nanoparticles are directly detected, most isotopes can be detected at picogram per milliliter (*ca.* 10 pg/mL) levels while some can be measured down to femtogram per milliliter (*ca.* 10 fg/mL) ranges, the mass detector possesses wide dynamic ranges (up to 9 orders of magnitude) and low matrix effects, excellent mass resolution and multielement detection of ICP-MS, and traceable absolute quantitative measurement [125]. Therefore, it is the most durable of all techniques, where MENPs can be measured in forms of particulates and even in dissolved ions, and does not have the equipment and safety restrictions of radioisotopes. MENPs can be detected at very low environmentally relevant concentrations with stable isotope labeling. In addition, there is likely no impact on MENPs properties, and it may be markedly useful in cases where organisms are chronically exposed to very low doses of MENPs or are in the food chain, although it may be more expensive than conventional method.

Imaging MENPs, *in vivo* or *ex vivo*, can provide direct information on their biodistribution and fate in organisms. Laser ablation-ICP-MS and secondary ion mass spectrometry could potentially be used for 2D imaging of stable-isotope-labeled MENPs in organisms, although their spatial resolution needs to be further improved [24,94,143].

3. Stable isotope labeling of carbon nanomaterials

3.1. Labeling protocols of carbon nanomaterials

The labeling of carbon nanomaterials by ^{13}C could be achieved by incorporating ^{13}C into the starting materials. There are very mature supply of ^{13}C-enriched organic molecules and carbon ash by commercial companies. The main efforts should be paid to perform the traditional protocols with ^{13}C-enriched carbon sources.

In the studies of the growing mechanism of carbon nanomaterials, ^{13}C-skeleton labeled CNTs were prepared by chemical vapor deposition (CVD) [133,135]. For example, Fan *et.al.* prepared various ^{13}C-labeled CNT samples by CVD method to reveal the growth mechanism of CNTs [135], in which ^{12}C- and ^{13}C-ethylene were introduced to CVD instrument in designed sequences and ratios to grow arrays of aligned CNTs containing intratube ^{12}C-^{13}C junctions on porous silicon substrate. A more applied method for ^{13}C-skeleton labeling of carbon nanomaterials is arc discharge method [130,132,144–146]. In the arc discharge method, the anode was filled by ^{13}C powder and the ^{13}C atoms reconstructed into carbon nanomaterials, such as C_{60}, CNTs, CQDs, carbon NPs and graphene. For instance, Chang *et al*. synthesized ^{13}C-skeleton labeled C_{60} and C_{70} from ^{13}C-enriched amorphous carbon powder by the arc-discharge method [130]. ^{13}C powder was filled into the graphite anode and the arc-discharge was performed at 110 A and 27 V. The ^{13}C-labeled fullerene samples were separated and purified through preparative HPLC. Alternatively, ^{13}C graphite power could be vapored by laser ablation. Sun and coworkers adopted the laser ablation of ^{13}C graphite power to obtain ^{13}C-labeled CNTs [134]. A mixture of powdery ^{13}C, graphite, Ni and Co with graphite cement were hot-pressed into a pellet, baked at 180 °C in air, cured at 810 °C and annealed at 1200 °C in argon flow to prepare the ablation target. The laser ablation of 10 Hz (2 J/pulse at 1064 nm and 9 mm beam diameter) was performed at 1150 °C with a steady argon flow. The soot was purified to obtain ^{13}C-labeled CNTs. The bottom-up synthesis and establishment of molecular structure model of carbon nanomaterials might be achieved using ^{13}C-enriched atomic carbon vapor or small carbon clusters [131,147,148]. In addition, the bottom-up synthesis strategy could be easily achieved by the hydrothermal treatment of small organic molecules, *e.g.*, ^{13}C-glucose, to prepare ^{13}C-labled CQDs [81].

3.2. Biological effects of carbon nanomaterials

Generally, carbon nanomaterials refer to fullerene and its derivatives, CNTs, graphene family nanomaterials (GFNs), graphdiyne, CQDs, carbon NPs and nanodiamonds [25,63]. Among them, the most studied carbon nanomaterials are sp^2 family. Fullerenes consist of 60 sp^2-hybridized carbon atoms arranged in a series of hexagons and pentagons to form a spherical structure, whereas CNTs are long tubular sp^2-hybridized structures. GFNs, which include graphene and graphene oxide (GO), consist of a single layer or a few layers of sp^2-hybridized carbon with a sheet-like structure. The sp^2 family shares similar structure with sp^2-hybridized carbon atom hexagons or pentagons. The ^{13}C stable isotope is incorporated into the skeleton carbon atom of these carbon nanomaterials and does not alter their stability and intrinsic structures [130,132,133,145]. Carbon nanomaterials in biological systems could be traced to the source and quantified with satisfactory sensitivity using ^{13}C-labeling [23,26,33,42,44,69].

The applications of ^{13}C-labeling in nanosafety evaluations were inspired by the success of ultrafine particles. In the early 2000, Prof. Günter Oberdörster and his colleagues investigated acute pulmonary effects of ultrafine particles in rats and mice [70,71]. The studies presented ultrafine particles more toxic than fine particles. They generated ultrafine carbon particles consisting of the stable isotope ^{13}C by using ^{13}C-graphite electrodes made in the laboratory from amorphous ^{13}C powder and carried on dosimetry studies with ultrafine ^{13}C-carbon particles. By using insoluble ^{13}C-carbon ultrafine particles, they determined the doses deposited in the respiratory tracts of laboratory animals, and quantified the extrapulmonary translocation of deposited ultrafine particles. The ultrafine carbon particles (20–29 nm) could translocate to the liver and other extrapulmonary organs following inhalation by rats. Since the natural abundance of ^{13}C is about 1.1%, they first tested the sensitivity of detecting added ^{13}C in organs by IRMS. Exposing each mouse to ultrafine ^{13}C particles (25 nm, ~100 μg/m^3) for 30 min or 6 h, the added lung burdens of ^{13}C after 30 min and 6 h of exposure were 82 and 199 ng, respectively. The sensitivity was sufficient to detect small amounts of accumulated ^{13}C in tissues. In subsequent studies, the added ^{13}C per gram of lung on average in the postexposure period was ~9 ng/g organ/μg/m^3 by using the method. Significant amounts of ^{13}C accumulated in the liver by 0.5 h post inhalation [71,72]. No significant increase in ^{13}C was detected in the other organs. Liver was an effective accumulation organ of ultrafine carbon particles by 1 d after inhalation exposure. The ultrafine ^{13}C particles showed the rapid initial clearance/translocation during an inhalation exposure of rats from the lower respiratory tract and then reached the blood circulation. Considering the lag-time effects and delay distribution of ultrafine particle, rats were exposure for 6 h. At 1, 3, 5 and 7 days postexposure, rats were sacrificed and lung, olfactory bulb, cerebrum, and cerebellum were removed for ^{13}C analysis. Through tracing the signal of ^{13}C, they proved that ultrafine carbon particles depositing on the olfactory mucosa of the nasal region translocated along the olfactory nerve into the olfactory bulb. Inhaled ultrafine carbon particles could translate into brain. Therefore, they proposed that the insoluble ultrafine ^{13}C-carbon particles were ideal for lung regional deposition dosimetry studies and for tracing ultrafine particle translocation to extrapulmonary organs.

Following the similar method, ^{13}C-labeling could be used for the *in vivo* quantification of carbon NPs. In 2014, Liu *et al*. reported that the biodistribution of carbon NPs in mice and its time-dependency [74]. Carbon nanoparticles can be quickly distributed to all organs of the body through the blood circulation and were mainly captured by mononuclear phagocyte system (MPS). Lungs, spleen, and liver of mice were their accumulation organs. Additionally, carbon nanoparticles suspension injection (CNSI) migrated

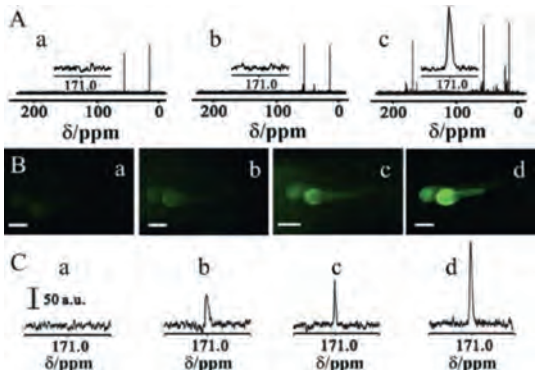

Fig. 1. (A) MR spectra of (a) zebrafish and the zebrafish incubated with 3.0 mg/mL, (b) ^{12}C-CQDs and (c) ^{13}C-CQDs. Inset: MR signal at around 171 ppm. (B) Fluorescent images and (C) MR spectra of zebrafish incubated with ^{13}C-CQDs at different concentrations, (a) 0, (b) 0.75, (c) 1.5 and (d) 3.0 mg/mL. Scale bar: 200 mm. Copied with permission [81]. Copyright 2014, Royal Society of Chemistry.

fast in lymphatic vessel and accumulated in sentinel lymph nodes, thus showed the high performance in tumor drainage lymph node (TDLN) imaging during oncological surgery. The direct accumulations of ^{13}C-CNSI in the first station (popliteal lymph node), the second station (common iliac artery lymph node), and the third station (paraaortic lymph node) of TDLN were 877 μg/g, 1062 μg/g and 405 μg/g, respectively, which explained the good imaging performance and provided quantitative approach to quantify CNSI in biological systems in future biomedical applications and biosafety evaluations [73].

The surface modification of carbon NPs did not affect the ^{13}C-labeling and quantification. For instance, carbon NPs showed bright fluorescence after preferably chemical functionalization with biocompatible organic molecules as CQDs. PEGylated ^{13}C-CQDs (with PEG_{1500N}) had strong fluorescence in aqueous solution (quantum yield of 20% at 440 nm excitation). According to IRMS analyses, the amounts of ^{13}C-CQDs in liver and spleen were much higher than those in other organs after intravenous injection. The biodistribution guided safety evaluations demonstrated that CQDs accumulations in liver and spleen did not arouse oxidative stress and toxicity *in vivo* [67,68]. In another pilot study, the detection of ^{13}C-labeled CQDs was achieved by magnetic resonance (MR). Yin *et al.* utilized ^{13}C-labeling to greatly enhance the MR signal of CQDs, where a 160-fold improvement on signal-to-noise ratio for the peak at around 171 ppm was achieved [81]. Carboxylated ^{13}C-CQDs were developed as MR and fluorescence dual-response probe for long-term observation of zebrafish embryonic development (Fig. 1), which provided specific information on the presence, magnitude, and progression of ^{13}C-CQDs by defining MR intensity, and fluorescence revealed the location of ^{13}C-CQDs with its high sensitivity. The ADME data of ^{13}C-QDs in zebrafish were obtained. CQDs selectively accumulated in the head, yolk sac, and tail. Zebrafish eye was the brightest part of head, which was confirmed by the MR responses along with the increased ^{13}C-CQD concentrations.

Fullerene shares similar shape of carbon NPs and CQDs, but had completely different structure as the first sp^2 carbon nanomaterials. Fullerene and its derivatives have been used in optical, electronic, cosmetic, and biomedical applications [29]. For the characterization and analysis of fullerenes in the real environment and living tissues samples, several analytical techniques including microscopy, spectroscopy, flow field-flow fractionation, electrophoresis, light scattering, liquid chromatography and mass spectrometry have been reported [57–63]. In 2014, Chang *et al.* developed ^{13}C-skeleton isotope labeling technique for the accurate quantification of trace amount of fullerene in biological systems [42]. The

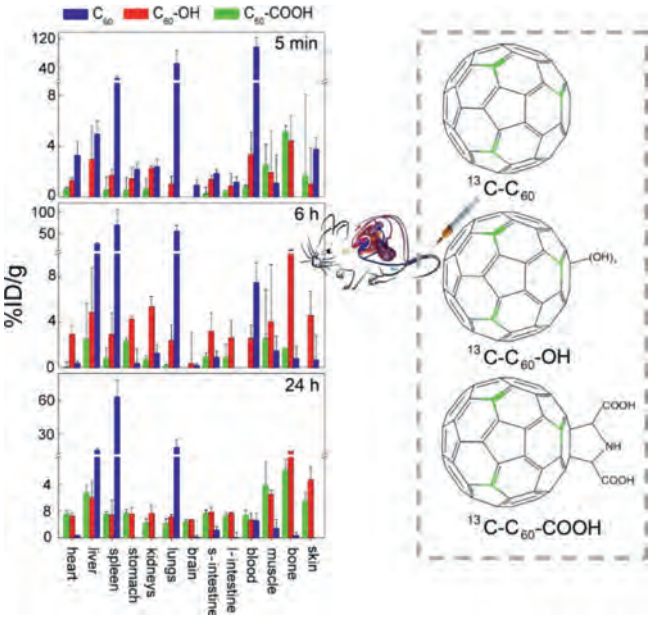

Fig. 2. Bioaccumulation of ^{13}C-C_{60} (pristine), ^{13}C-C_{60}-COOH (carboxylated) and ^{13}C-C_{60}-OH (hydroxylated) in mice after intravenous injection. Copied with permission [75]. Copyright 2016, Wang *et al.*

cage skeleton carbon atoms of fullerene C_{60} were substituted by stable ^{13}C isotope for the quantification of *in vivo* ADME in mice. According to the IRMS measurement, ^{13}C-C_{60} was cleared quickly from the blood stream following the two-compartmental model and transported to all organs of mice. Live, spleen and lung were the main accumulation organs at 24 h post-exposure. Liver was the main metabolic organ of ^{13}C-C_{60}. ^{13}C-C_{60} rapidly entered the liver within 5 min and reached the maximum absorption at 6 h. With the extension of time, the hepatic content decreased slightly and still accumulated within 24 h. Another use of ^{13}C isotope was the internal standard. Internal standard quantification using stable isotope labeled internal standards is de rigueur for trace level analysis of organic contaminants in environmental matrices [58]. Isaacson *et al.* added $^{13}C_{60}$ as an internal standard during the quantification of fullerene (from C_{60} to C_{98}) by liquid chromatography/electrospray ionization mass spectrometry [58]. The quantification data guided the *in vivo* toxicity assays of fullerenes in embryonic zebrafish.

The well-defined structure of fullerene allows the precise investigation of impact of its surface modification, which plays an essential role in improving the biocompatibility, regulating the *in vivo* distribution and metabolism, and alleviating the toxicity [149]. Stable ^{13}C-skeleton labeled technique is a powerful tool for this purpose. Chang *et al.* generated ^{13}C-C_{60} (pristine), ^{13}C-C_{60}-COOH (carboxylated) and ^{13}C-C_{60}-OH (hydroxylated) and compared firstly their biodistribution following three routs of administration [75]. The liver, bone, muscle and skin were found to be the major accumulation organs for C_{60}-COOH and C_{60}-OH after intravenous injection, whereas unmodified C_{60} was mainly found in the liver, spleen and lung (Fig. 2). The total uptakes in liver and spleen followed the order: C_{60} >> C_{60}-COOH > C_{60}-OH. The distribution rate over 24 h followed the order: C_{60} > C_{60}-OH > C_{60}-COOH. Both C_{60}-COOH and C_{60}-OH were cleared from the body at 7 d post exposure. C_{60}-COOH was absorbed in the gastrointestinal tract following gavage exposure and distributed into the heart, liver, spleen, stomach, lungs, intestine, and bone tissues. The translocation of C_{60}-OH was more widespread than that of C_{60}-COOH after intraperitoneal injection. The surface modification of fullerene C_{60} led to decreases of accumulation levels and distribution rates, as well as

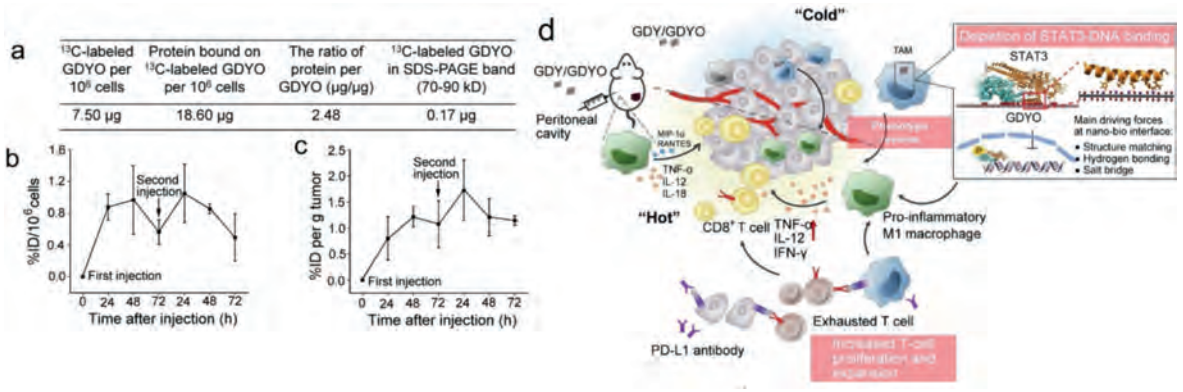

Fig. 3. Characterization of the intracellular protein corona on GDYO nanosheets by ^{13}C-labeled GDYO. (a) The protein adsorption capacity was calculated as the mass of the protein adsorbed *versus* the mass ratio of protein to GDYO material. (b) Cellular uptake by macrophages. (c) Tumor uptakes of GDYO after double injections (100 μg/injection). (d) Schematic overview of the mechanism whereby graphdiyne oxide nanosheets reeducate immunosuppressive macrophages through the intracellular corona, facilitating cancer immunotherapy. Copied with permission [80]. Copyright 2021, American Chemical Society.

the alteration of accumulation organs. The distribution information obtained by ^{13}C-labeling directly demonstrated that the chemical functionalization had significant impacts on the translocation and biodistribution behaviors of carbon nanomaterials.

Other sp^2 carbon nanomaterials were also labeled by ^{13}C isotope for bio-effect studies. In 2007, Yang *et al.* reported that the skeleton ^{13}C-enriched single-walled CNTs (SWCNTs) could be prepared by laser ablation method and quantified by IRMS after they were intravenously injected in mice [49]. SWCNTs were distributed in the entire body, with major accumulations in the liver, lungs, and spleen over an extended period of time. Furtherly, the pharmacokinetic and biodistribution of PEGylated SWCNTs in mice were quantified by ^{13}C-labeling [47]. The lower hepatic uptake of PEG-SWCNTs was observed with an ultra-long blood circulation. The results indicated that covalent PEGylation of SWCNTs was the most effective approach to prolong their blood circulation, which led to the meaningful tumor uptake by enhanced permeability and retention (EPR) effect. ^{13}C quantification results suggested the potential applications of the stealth CNTs in the drug-delivery and other biomedical systems [50–52].

More recently, ^{13}C-labeling was extended to quantify graphdiyne [80]. Graphdiyne oxide (GDYO) is a novel two-dimensional (2D) carbon nanomaterial comprising of hybridized sp^2 and sp carbon atoms. GDYO is potentially useful in energy storage, electrocatalysis and biomedicine [150,151]. The surfaces of GDYO nanosheets are consisted of well-arranged C=O and C–OH groups. These groups have a high affinity for proteins that is driven by hydrogen bonding and the formation of salt bridges. Chen and Chang took advantage of ^{13}C-GDYO to confirm the GDYO-bio interaction at tissue, cell, and molecular levels (Fig. 3). The interaction mechanism between the GDYO-protein interface included the formation of intracellular protein corona consisting of signal transducer and activator of transcription 3 (STAT3), inducing the reeducation of immunosuppressive macrophages in cancer immunotherapy.

3.3. Environmental effects of carbon nanomaterials

STable ^{13}C isotope labeling technique is also applied to evaluate the environmental risk by studying the behavior and occurrence of carbon nanomaterials at low concentrations in natural environmental samples [55]. The labeling and analytical methods are similar to those in bio-effect studies.

The bioaccumulation of ^{13}C-fullerenol nanoparticles in wheat was investigated firstly by Chang and coworkers [44]. The dose and time dependent bioaccumulation of fullerenol in wheat seedlings

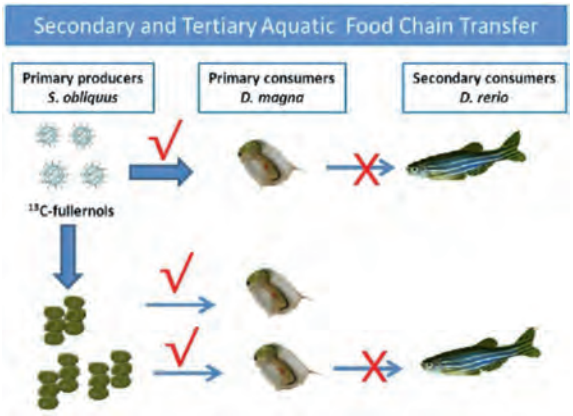

Fig. 4. Trophic transfer and biomagnification of ^{13}C-fullerenol nanoparticles in aquatic food chain, red Yes√: BMF > 1; red No × : BMF < 1. Copied with permission [43]. Copyright 2018, American Chemical Society.

was observed. The majority of fullerenol (85.68-263.86 %ID/g) were only found in the roots and very limited amounts (4.13 %ID/g) translocated to the stems and leaves. The presence of fullerenol in leaves enhanced the photosynthesis rate and the growth of seedlings. ^{13}C-C_{60} were absorbed in rice seedlings roots and affected the seedling growth by regulating the phytohormone levels [76]. These works started the foundations for the quantitative, safe, and non-destructive evaluation of the environmental fate of carbon nanomaterials. Subsequently, the bioaccumulation, biodistribution, depuration, trophic transfer and biomagnification of ^{13}C-fullerenol nanoparticles in three-level aquatic food chain (*Scenedesmus obliquus* to *D. magna* to *Danio rerio*) were systematically investigated [43,45,46,77]. The fullerenol nanoparticles accumulated in *S. obliquus* through water exposure, and the latter was ingested by *D. magna* before being transferred to *D. rerio* (Fig. 4). The tissues of *D. rerio* were ranked from highest to lowest fullerenol concentration as follows: intestine > liver > muscle > gills > brain. The biomagnification factor (BMF) value of fullerenols from *S. obliquus* to *D. magna* was 3.20, while the fitted BMF from *D. magna* to *D. rerio* was less than 1 ($BMF_f = 0.54$). Fullerenols were significantly biomagnified from the first to the second trophic level, but not from the second to the third trophic level. ^{13}C-fullerenol nanoparticles could be enriched in *S. obliquus*. The maximum concentration of ^{13}C-fullerenols in *S. obliquus* exposed to 1.0 mg/L ^{13}C-fullerenols was attained at 2 d, reaching 26.7 mg ^{13}C-fullerenols/g dry weight algae. The algae suppressed

the uptake of fullerenols by *D. magna*. The capacity of *D. magna* to ingest fullerenols *via* the aqueous route was much higher than that *via* the dietary route. After exposure to ^{13}C-fullerenols in artificial freshwater for 48 h, the steady concentrations of fullerenols in *D. magna* were nearly 0.39% and 1.37% of the dry body weight in the 0.1 and 1.0 mg/L exposure groups, respectively. After 48 h of depuration, *D. magna* could excrete 97.34% and 89.56% of the accumulated fullerenols in the 0.1 and 1.0 mg/L exposure groups, respectively. The depuration of fullerenols from *D. magna* followed the first-order kinetics. Moreover, the accumulated fullerenols in gravid *D. magna* could be transferred to the next generation of neonates. The uptake, bioaccumulation, biodistribution, depuration, and uptake-depuration kinetics of ^{13}C-fullerenols in zebrafish through a dietary exposure pathway were also quantitatively investigated. After exposure to ^{13}C-labeled fullerenol solution at a concentration of 2.5 mg/L for 72 h, the steady state concentration of fullerenols in *D. magna* was 31.20 ± 1.59 mg/g dry weight. During the 28-d uptake period for zebrafish, fullerenols in the tissues increased in a tissue- and day-dependent manner, and the major accumulation tissues of fullerenols were the intestine and liver, followed by the gill, muscle, and brain. After depuration for 15 d, a certain amount of residual fullerenols remained in the tissues, especially the brain, where approximately 64 d may be needed to achieve 90% of the cumulative concentration depuration. The calculated distribution based on trophic transfer factors (TTF_d values) (from 0.26 to 0.49) indicated that the tissue biomagnification of fullerenols by zebrafish through dietary exposure might not occur, which confirmed that there was no risk of tissue biomagnification in zebrafish. These works showed more complete data from primary producers to secondary consumers to top consumers of a three-level aquatic food chain, which benefited to environmental and ecological risk assessments of carbon nanomaterials. Stable isotope ^{13}C-labeling was proven as a powerful tool to both quantify directly carbon nanomaterials without complex sample extraction processes which distinguished between endogenous and exogenous carbon nanomaterials, and investigate the environmental fate and the potential impacts of carbon nanomaterials in ecological systems. Furtherly, Chang and coworkers developed a novel method to *in situ* visualize the localization and spatial distribution of fullerenol nanoparticles in organisms using LA-IRMS and matrix-assisted laser desorption/ionization imaging mass spectrometry (MALDI-IMS) [82]. LA-IRMS with high spatial resolution down to 50 μm allowed the image analysis of carbon isotope (^{13}C) signature in organism samples indirectly. Matrix assisted laser desorption ionization time-of-flight mass spectrometry (MALDI-TOF-IMS) with the smallest laser spot size (1 μm) enables the imaging of target directly with subcellular spatial resolution.

Other groups also reported the ^{13}C-labeling of fullerene in environmental risk assessments. Schreiner *et al*. reported the first evidence of ^{13}C-fullerenol biodegradation and utilization in microbe using ^{13}C IRMS technique [85]. After 32 weeks of decay, white rot basidiomycete fungi could bleach and oxidize fullerenol to CO_2, and incorporate it into fungal biomass according to the gas chromatographic analysis of fatty acids. However, Wiesne *et al*. found that ^{13}C-labeled C_{60} was difficult to be degraded into CO_2 by microorganisms [86]. The size of C_{60} aggregates decreased, while the hydroxylation and photosensitized reactivity increased after microbial culture for 24 months. The interactions of abiotic photochemical transformations of $^{13}C_{60}$ and its subsequent biotic mineralization in soil were investigated furtherly [83,84]. C_{60} addition altered soil microbial community composition during the duration of C_{60} photo-irradiation. Excess ^{13}C in the respired CO_2 demonstrated that photo-irradiating enhanced the C_{60} microbial degradation in soil. The abiotic and biotic transformation process of microenvironment would potentially influence the degradation of carbon nanomaterials in the natural environment. Coupled photochemical and microbial mineralization dynamics would be a facile mechanism of decomposition of C_{60} in an environmental release. Soil microcosms rapidly mineralized fullerenol carbon, as determined by ^{13}C content in the respired CO_2. By tracking the enriched ^{13}C from fullerenol into microbial phospholipid fatty acids (PLFA), we also reported the incorporation of nanomaterial-derived C into soil microbial biomass, primarily by fungi and Gram-negative bacteria. In contrast to pristine C_{60}, surface functionalized C_{60} (fullerenol) was readily mineralized by a range of soil microorganisms.

^{13}C-labeling is applicable in the environmental toxicity evaluations of other carbon nanomaterials. Hanna *et al*. used carbon stable isotope ratios of carbon nanotubes (CNTs) to examine the toxicity, fate and transport of CNTs in marine mussels after exposure to 1.0, 2.0 and 3.0 mg/L of CNTs for four weeks [87]. CNTs accumulated in marine mussels. Mussels decreased the clearance rate of phytoplankton by 24%. Mussel growth rate was unaffected by CNT concentrations up to 3 mg/L. Mussels deposited most CNTs in biodeposits, which contained >110 mg/L dry weight, and accumulated about 1 mg/L dry weight of tissue. The deposition of highly concentrated feces and pseudofeces into benthic environments would impact infaunal organisms living in and around mussel beds. Chang and coworkers utilized ^{13}C-stable isotope to skeleton label GO and investigated its bioaccumulation and toxicity in wheat seedlings [79]. ^{13}C-GO predominantly accumulated in the root with a content of 112 μg/g at day 15, hindered the development and growth of wheat plants, disrupted root structure and cellular ultrastructure, and promoted oxidative stress. Subsequently, using ^{13}C-skeleton-labeling technique, the translocation of two graphene materials was quantified in pea seedlings [78]. The chemical reduction of GO enhanced the *in vivo* translocation and photosynthetic inhibition (Fig. 5). The reduced GO (RGO) was translocated more easily from roots into leaves and directly inhibited the activity of photosystem II by damaging the oxygen-evolving-complex on the donor side. The toxicological mechanism was attributed to oxidative stress. These results revealed the relationship between the structure of graphene nanomaterials and their environmental bio-effects, environmental biosafety and biological effects, which would benefit the understanding of their biosafety and the design of environment-friendly graphene products.

4. Stable isotope labeling of metal/metal oxide nanomaterials

4.1. Labeling protocols of metal/metal oxide nanomaterials

In the use of stable isotope labeling for MENPs, MENPs are labeled by enriching a stable isotope of the relevant metals that exists at low abundance in the environment. The preparation of enriched stable isotope MENPs is achieved by synthesis with a stable-isotope-labeled precursor of the relevant metal-based materials. Thus, the main efforts should be paid to the stable-isotope-labeled precursor. Generally, the enriched precursors are commercial as solid metals, solid metal oxides or other soluble salt complexes [53,124,127].

There are three main methods for producing stable isotopes precursors, namely distillation, centrifugal concentration and electromagnetic concentration (calutron) [152]. Distillation is only used to separate isotopes of light elements, such as He, Li, B and C. Centrifugal concentration is the most cost-effective method for separating isotopes of heavy elements, such as Fe, Ni, Zn, Cd, Ge, Se, Te and W. The calutron is capable of enriching isotopes of almost all elements, but it is expensive and only produces relatively small amounts in the isotope production of Tl, Pd, Sr, Ca and the Lanthanide group. Other methods, such as laser enrichment, photo-chemical enrichment and plasma separation, are seldom used at present. Current producers have shown that the type,

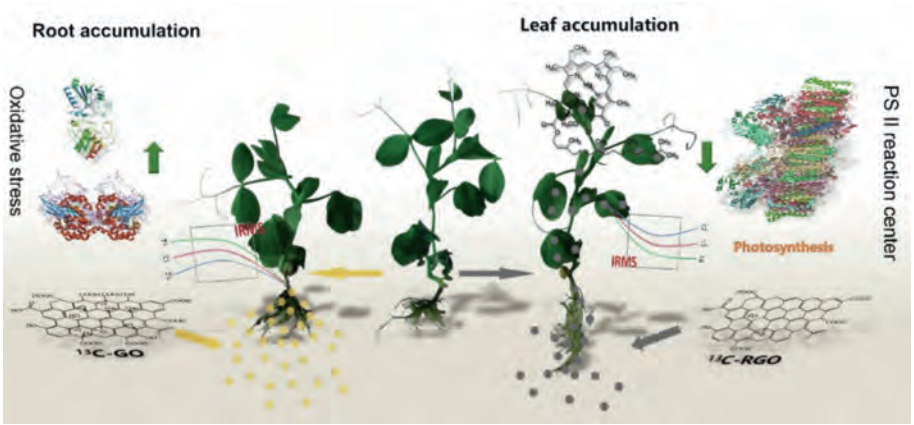

Fig. 5. Schematic diagram of chemical reduction of graphene enhances *in vivo* translocation and photosynthetic inhibition in pea plants. Copied with permission [78]. Copyright 2019, Royal Society of Chemistry.

natural abundance (%) and the enrichment available concentrations (%) of stable isotopes of the different enriched precursors. Many stable isotopes have been successfully employed in the study of the enriched precursors (Table S1 in Supporting information).

To select proper stable isotope for labeling MENPs, some elements are not recommended: (1) The element has only one stable isotope, such as Beryllium (^{9}Be), Sodium (^{23}Na), Aluminum (^{27}Al), Scandium (^{45}Sc), Manganese (^{55}Mn), Cobalt (^{59}Co), Arsenic (^{75}As), Yttrium (^{89}Y), Niobium (^{103}Nb), Rhodium (^{103}Rh), Gold (^{197}Au). (2) The stable isotope element is not suitable for tracing because of its large natural abundance, such as Lithium (^{7}Li), Magnesium (^{24}Mg), Silicon (^{28}Si), Potassium (^{39}K), Calcium (^{40}Ca), Chromium (^{52}Cr), Iron (^{56}Fe), Nickel (^{58}Ni), Zinc (^{64}Zn), Cerium (^{140}Ce). (3) The enriched isotope is strongly interfered during the sampling or measurement. Since isotope ratios or concentrations will be measured at very low concentrations, even with collision/reaction cell techniques, minor interferences can affect the accuracy of results. For example, ^{50}Ti and ^{49}Ti are not suitable tracers for TiO_2 due to the polyatomic interferences $^{36}Ar+^{14}N$ and $^{32}S+^{16}O+^{1}H$. Instead, ^{47}Ti can be chosen as a tracer to avoid interferences and to obtain accurate isotopic ratios in labeled MENPs [105]. (4) The stable isotope is strictly regulated. For example, ^{6}Li is used in thermonuclear weapons, thus not available in the export and use. Notably, these stable isotopes have a number of other special situations and uses. (5) The stable isotope is converted into other elements for applications. For example, ^{48}Ti (natural abundance of 73.7%) is used for the production of the radioisotope ^{48}V for nutritional studies and calibrating PET instrumentation. ^{63}Cu (natural abundance of 69%) is used for the production of medical radioisotope ^{62}Zn and ^{64}Cu.

There is an exceptional that the element contains two stable isotopes close to 50% natural abundance. Such as ^{107}Ag (natural abundance of 51.4%) and ^{109}Ag (natural abundance of 48.7%), ^{121}Sb (natural abundance of 57.2%) and ^{123}Sb (natural abundance of 42.8%). The double stable isotope tracing is a common method to study the intracellular dissolution of silver nanoparticles. For example, Yu *et al.* [15] co-cultured HepG2 and A549 cells with two enriched stable Ag isotopes (^{107}AgNPs and $^{109}AgNO_3$) at nontoxic doses to track the transformations of Ag NPs *in vivo*.

4.2. Labeled metal/metal oxide nanomaterials for nanosafety researches

In recent years, stable isotope labeling has been developed as an alternative technique for tracking the behavior of MENPs in environmental and biological systems. Stable isotope ratios can be measured by conventional ICP-MS (*e.g.*, quadrupole ICP-MS) or high-resolution ICP-MS/MC-ICP-MS, which provide very sensitive signals that distinguish them from endogenous background metals in various samples [65,124,154,155]. For example, typically using quadruple ICP-MS, $^{107}Ag/^{109}Ag$ ratios can usually be measured with an accuracy of no more than 1%. However, improved precision data for $^{107}Ag/^{109}Ag$ can be obtained in excess of 0.02% by using MC-ICP-MS and effective purification techniques [90]. Thus, the application of stable isotope labeling improves the tracer sensitivity by a factor of at least 40 (for quadruple ICP-MS) and possibly by a factor of about 4000 (for MC-ICP-MS). To this regard, the high-precision MC-ICP-MS is very promising in quantifying the low exposure concentrations of MENPs in environmentally or toxicologically realistic scenarios.

Metal stable isotope labeling especially multi-isotope labeling combined with high-precision mass spectrometry mainly as MC-ICP-MS provides a new opportunity to identify the contribution of ions and particles to the bioavailability of MENPs. Zn and its isotopes are the most studied ones in isotope labeling of MENPs. Taking Zn as an example, stable isotope labeled ZnO NPs could be quantified during the environmental toxicity studies. Khan *et al.* studied the waterborne uptake and efflux kinetics of aqueous ^{68}Zn, ^{68}ZnO NPs and ^{68}ZnO bulk particles by estuarine snail (*Peringia ulvae*). The solubility of ZnO NPs in the exposure media was a key parameter that determined the bioavailability of the Zn constituent [156]. Laycock *et al.* further employed double stable isotope labeled ^{68}ZnO NPs and soluble $^{64}ZnCl_2$ to test the bioavailability of ZnO NPs in earthworms through soil exposure. Based on the dual-isotope tracer $^{68}Zn/^{64}Zn$ ratios of earthworms, soils, and pore waters, they proved directly that the rapid dissolution of ZnO NPs was the most likely explanation for the indistinguishable environmental distribution and uptake of Zn ions and particles [157,158]. The $^{68}Zn_{en}/^{64}Zn_{en}$ ratios were quite similar for earthworms (1.09 ± 0.04), soils (1.09 ± 0.02) and pore waters (1.08 ± 0.02) (Fig. 6). Likewise, Caldelas *et al.* used Zn stable isotope ($^{68}Zn/^{66}Zn/^{64}Zn$) mass balance methods to distinguish the uptake of particles and ions in wetland plants [159]. Four ZnO materials of micron-size ZnO, nanoparticles (NPs) of $<$100 nm or $<$50 nm, and nanowires of 50 nm diameter were studied in the uptake and phytotoxicity to *Phragmites australis* by combining Zn stable isotopes and inductively coupled plasma optical emission spectrometry (ICP-OES). Nanoparticles of $<$50 nm released more Zn^{2+} and were more toxic, which led to the greater Zn precipitation and accumulation in the roots and the decrease of Zn isotopic fractionation. Exposure to ZnO nanomaterials took place mostly through the uptake of dissolved Zn^{2+}, but also through direct contact with the root surface.

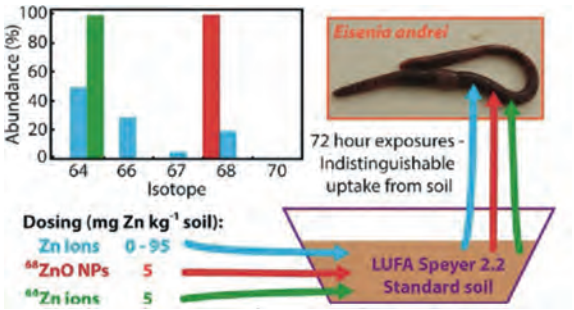

Fig. 6. Schematic diagram of novel multi-isotope tracer approach to test ZnO nanoparticle and soluble Zn bioavailability in joint soil exposures. Copied with permission [158]. Copyright 2017, American Chemical Society.

The human body contains a high Zn background, and it is difficult to identify the relatively small amount of exogenous Zn in body. The advantages of metal stable isotope labeled ZnO NPs enable the direct quantification of ZnO in such a high background. Gulson *et al.* [95] enriched ZnO with stable isotope ^{68}Zn to > 99%, and distinguished the skin zinc absorbed from naturally occurring zinc. Small amounts of zinc contained in ZnO particles of sunscreen penetrated the protective layer of skin to be detected the blood and urine. In follow-up trials, over a 50-day long period of exposure, blood Zn levels continued to increase after 5 days, peaking at 14 days after first use with a low level of zinc absorption by the skin (minimum estimate less than 0.01% of the applied dose) [96]. Their study established that ^{68}Zn stable isotope labeling combined with high-precision isotope ratio measurements by MC-ICP-MS can effectively track zinc in human skin exposed to ZnO NPs in complex media of high zinc background [97]. In addition, Osmond-Mcleod *et al.* [99] found that the concentration of ^{68}Zn in organs of virgin mice treated with sunscreen containing ^{68}ZnO NPs was significantly higher than that of mice treated with sunscreen containing larger ^{68}ZnO particles. Moreover, the time-of-flight secondary ion mass spectrometry (TOF-SIMS) and confocal laser scanning microscopy (CLSM) imaging method were developed for rapid and sensitive cytotoxicity study of ZnO NPs using human skin HaCaT cells as a model system. Additional validation by using stable isotope-labeled ^{68}ZnO NPs as tracers under the same experimental conditions yielded similar cytotoxicity effect [98]. This suggested that the stable isotope labeling did not affect the bio-effects of MENPs.

The natural abundance of stable isotopes determined the sensitivity and selectivity of isotope labeling. Using isotopes of lower abundance usually provides better quantification sensitivity and accuracy. There are five stable isotopes of Zn that differ widely in their natural abundance: ^{64}Zn (48.9%), ^{66}Zn (27.8%), ^{67}Zn (4.1%), ^{68}Zn (18.6%) and ^{70}Zn (0.3%). The natural abundance of ^{67}Zn (4.1%) is smaller and tends to be more sensitive. Stable isotope technique is sufficiently sensitive to determine the uptake of Zn at an exposure equivalent to a lower concentration range (<15 μg/g) of environmentally realistic exposure conditions [100]. Buffet *et al.* used ^{67}ZnO NPs to trace the fate of NPs in sediments and investigated bio-uptake in two estuarine intra-sedimentary invertebrates *Scrobicularia plana* and *Nereis diversicolor* [101]. ^{70}Zn (0.3%) also has a high sensitivity due to its lowest natural abundance. Nath *et al.* [92] reported that the absorption/retention of ^{70}ZnO NPs was greater in roots than in shoots in *Arabidopsis thaliana*. Zn was found in the root tissues of plants, but not in the form of NPs.

Following similar concept in stable isotope labeling of Zn containing NPs, MENPs could be labeled and quantified by using other stable isotopes, too. Another widely concerned category is Ag NPs, which are inevitably released into the environment due to the mass production and wide use [55,93,128,153]. Stable isotope labeling technique is irreplaceable in the environmental and biosafety evaluation of Ag NPs. Gigault and Hackley [88] studied the estuarine sediments by doping Ag NPs with known quantities of isotope ^{109}Ag. Ag NPs interacted with different grain components of the sediment and self-associated to form clumps in the model estuarine system. Croteau *et al.* [89] labeled the citrate coated Ag NPs by ^{109}Ag (isotope abundance of 99.7%) and quantified the bioaccumulation of Ag NPs in freshwater snails. Without labeling, Ag NPs were undetectable. With ^{109}Ag labeling, at 6 ng/L and higher, Ag was detected in *Lymnaea stagnalis*, where more than 70% of detected Ag was from the newly dissolved Ag^+. The organisms showed the tolerance to Ag, but were more sensitive to Ag NPs in the diet. Laycock *et al.* reported that ^{107}Ag-enriched particles were indistinguishable in size and shape from particles with natural isotopic composition [90]. Isotope mass balance calculations showed ^{107}Ag labeling increased the Ag NP tracking sensitivity by at least 40 times. Nath *et al.* [92] quantified ^{107}Ag NPs in *A. thaliana*. The absorption/retention of Ag NPs in roots was more than in stems. Analyses by single particle ICP-MS and scanning electron micrographs (SEM) equipped with energy dispersive spectroscopy (EDS) proved the presence of Ag NPs in roots.

During the environmental behavior studies, the transformation between Ag NPs and Ag^+ is difficult to study by traditional methods, but double stable isotope labeling method provides meaningful insights. The stable isotopes of silver have similar abundance, namely ^{107}Ag (51.4%) and ^{109}Ag (48.7%). Yu *et al.* [91] used two stable Ag isotopes in the same experiment to track the transformation kinetics of ^{107}Ag NPs (isotope abundance of 99.5%) and $^{109}Ag^+$ (isotope abundance of 99.81%) in aquatic environment. The dissolved Ag^+ (^{109}Ag) could be distinguished from Ag^+ (^{107}Ag) already in solution by ICP-MS. The conversion between Ag NPs and Ag^+ was quite complicated and largely depended on external conditions, such as temperature, pH and cations. Zhang *et al.* prepared ^{107}Ag NPs of unique isotopic composition for the oxidation study [56]. When Ag NPs were released into the environment, they were oxidized to release Ag^+. Subsequently, the released $^{107}Ag^+$ and preexisting $^{109}Ag^+$ could be reduced to produce a mixed source of regenerated Ag NPs with different isotopic composition. Yang *et al.* [93] used dual stable isotope tracers ($^{107}AgNO_3$ and ^{109}Ag NPs) to identify the absorption and transformation of Ag NPs and ions in rice plants. Ag NPs were directly absorbed by roots, and the higher proportion of Ag^+ ions in stems indicated that Ag NPs were oxidized *in vivo*. Shao *et al.* [94] studied the transfer and transformation of intracellular and intercellular Ag NPs in oyster gill filaments by coupling nanoscale secondary ion mass spectrometry (NanoSIMS) and dual stable isotope tracing (^{109}Ag NPs and $^{107}Ag^+$ ions). ^{109}Ag hotspots were found to be co-located with endosomes or lysosomes, suggesting that Ag NPs entered the oyster through endocytosis by the gill epithelial barrier. These ^{109}Ag hotspots showed a strong colocalization with $^{32}S^{2-}$.

The situation is trickier for Ce-containing NPs. Stable Ce isotope has a high natural abundance, thus it is not suitable for isotope tracing. Commercially Ce containing NPs do not have a distinct isotope signature and their detection in natural samples is not feasible by stable isotope tracing. Based on mass dependent differences in the Ce stable isotope compositions (^{142}Ce/^{140}Ce), Laycock *et al.* developed one promising tracing approach for the precise determination of the ^{142}Ce/^{140}Ce isotope ratio by MC-ICP-MS using Ba for external normalization of the instrumental mass bias. They exploited the isotopic signatures in many kinds of commercial CeO_2 nano- and bulk-particles and other purified Ce materials [102]. The method offered the reproducibility (2sd) of about ±0.05‰, and the precisions of ±0.01‰ (2se) and ±0.04‰ (2sd), which should still be applied if an enriched Ce isotope was used to produce isotopically labeled CeO_2 NPs. Similarly, Praetorius *et al.* took advantage of mass dependent differences in the stable isotope composi-

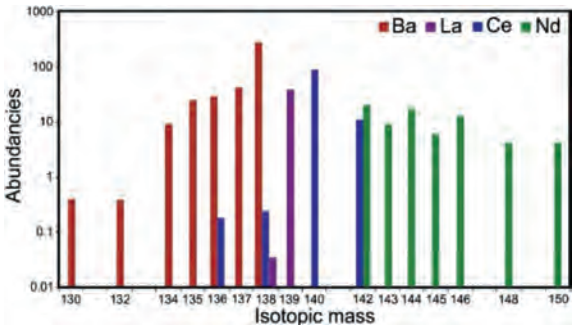

Fig. 7. Ce, Nd, La and Ba isotope abundances normalized to the primitive mantle elemental abundances. Copied with permission [104]. Copyright 2019, Royal Society of Chemistry.

tions of elements to present a groundbreaking new approach using an inductively-coupled plasma time-of-flight mass spectrometer (ICP-TOF-MS) in single-particle mode. The new method was capable of simultaneous multi-element analysis, coupled with a machine learning data treatment [103], which was successfully applied to distinguish engineered CeO_2 NPs (CeO_2 ENPs) from natural Ce-containing NPs (Ce-NNPs) in soils at low environmental ENP concentrations. Further, Bonnand *et al.* separated Ce from silicate matrices for the analysis of radiogenic (ε^{138}Ce) and mass dependent (δ^{142}Ce) Ce isotope variations by TIMS [104]. The method associated with 10^{13} Ω amplifiers that allowed the precise determination of the ^{140}Ce peak tailing effect on the lighter Ce isotopes and the reduction of the counting time necessary to obtain a high precision isotopic composition. The best reproducibility for δ^{142}Ce was about ±0.028‰. The method allowed the simultaneous measurement of the four Ce isotopes and their isobaric interferences (^{134}Ba, ^{139}La and ^{143}Nd) together with intercalated masses for tailing correction (Fig. 7). It is fundamental to perfectly isolate Ce from the matrix and isobaric interference elements in order to produce accurate and precise mass dependent stable Ce isotope measurements.

TiO_2 NPs are widely used in sunscreen with ZnO NPs. The stable isotope ^{47}Ti has been adopted in quantifying TiO_2 NPs. Bourgeault *et al.* reported that the assimilation efficiency (AE) of mussels to $^{47}TiO_2$ NPs was very low (3.0% ± 2.7%) [105]. $^{47}TiO_2$ NPs were mainly captured in the mussel gut and rarely penetrated into their internal organs. Similarly, Zhang *et al.* [56] reported the newly accumulated Ti in mussels (0.2 μg/g), which were exposed to $^{47}TiO_2$ nanomaterials at an environmentally relevant concentration of 3.9 μg/L.

Iron is essential element and holds high backgrounds in the environment and organisms. To study the trace changes induced by Fe containing NPs, stable isotope labeling is very suitable to distinguish from the background. As early as 1985, Eagles *et al.* [160] had used stable isotope ratio mass spectrometry to study the bioavailability of iron ($^{58}FeSO_4$, isotope abundance of 72.18%) by measuring the changes of ^{58}Fe/^{56}Fe ratio. Handler *et al.* measured the degree and rate of Fe isotope exchange between aqueous Fe(II) and goethite nanorods using ^{57}Fe isotope tracer. Almost complete exchange of Fe atoms between the aqueous phase and goethite nanorods was observed over a period of 30 days by monitoring the ^{57}Fe/^{56}Fe ratio changes. During the incubation, aqueous $^{57}Fe^{2+}$ exchanged with Fe(II) of goethite nanorods, resulting in the continuous increase of ^{57}Fe/^{56}Fe ratios for goethite nanorods [106]. Meermann *et al.* [107] coated iron oxide NPs (^{57}Fe) with SiO_2 shell ($^{57}Fe@SiO_2$ NPs). Explicit tracing of $^{57}Fe@SiO_2$ NPs between natural iron colloid grades was achieved despite the high background of "natural" iron. The quantification of $^{57}Fe@SiO_2$ NPs in sediment slurry matrix could be achieved by measuring ^{57}Fe/^{56}Fe ratios. The limit of quantification was 7.8 μg/L and the limit of detection was 2.4 μg/L in sediment slurry matrix.

Cu is another essential element and the stable isotope labeling of Cu containing NPs has been reported. Misra *et al.* [108] determined the uptakes of CuO NPs at exposure concentrations equal to background copper concentrations in freshwater systems (0.2–30 μg/L). Without tracers, the newly accumulated Cu was undetectable even at concentrations greater than 1 mg/L due to the high Cu background of 34 μg/g in *L. stagnalis*. With ^{65}Cu tracers, it was observed that the net ^{65}Cu uptake increased linearly along with the exposure concentration increases (<150 ppb). Croteau *et al.* [109] investigated the processes controlling bioaccumulation of CuO NPs in freshwater snails following exposure to aqueous system and diet containing ^{65}Cu-labeled CuO NPs. The association between bioaccumulation and toxicity after exposure to CuO NPs was established. Uptake rates of ^{65}Cu into *L. stagnalis* increased linearly with ^{65}CuO NP concentrations (<300 nmol/L). The k_{uw} was 0.31 L g^{-1} d^{-1} after waterborne exposure. The increase of ^{65}CuO NP uptakes was also linearly during dietary exposure. The k_{uf} was 0.13 g g^{-1} d^{-1}. However, Cu-laden diatoms showed the uptake decreases at >10,000 nmol/g. The Cu assimilation efficiency was higher for CuO NPs than Cu-laden diatoms. Dietary exposure to CuO NPs was more likely to cause adverse effects than waterborne exposure. Nath *et al.* [92] found that ^{65}Cu NPs were suitable for tracing in plants. ^{65}Cu NPs led to more ^{65}Cu uptakes in roots than shoots of *A. thaliana*.

5. Stable isotope labeling in drug development

Beyond the aforementioned safety issues, stable isotope labeling showed great potential in drug development. Traditional drug development has used stable isotope tracing to assess tumor metabolism, *e.g.*, ^{13}C-glucose [141]. Even at the beginning of nanosafety researches, scientists paid great attention to the positive bio-effects of nanomaterials that have potentials in biomedical applications, such as fullerene derivatives and CNTs [42,47–49,75]. To develop nanomedicine, the pharmacokinetics and ADME data are essential for the biosafety evaluation of nanomedicine in preclinical studies. The targeting efficiency and persistent retention of nanomedicine in targets also require the quantitative information of nanomaterials. In addition, once the nanomedicine goes into clinical trials, the quantification of nanomaterials in tissues and excreta is required [140].

Recently, we established an example of stable isotope labeling guided nanomedicine development. Carbon nanoparticle suspension injection (CNSI) is a commercially applied staining reagent for sentinel lymph node mapping in oncological surgery [161,162]. To expand the clinical applications of CNSI into drug delivery [163,164] and photothermal therapy [165], the National Medical Products Administration of China requires the ADME data of CNSI. We adopted the arc discharge method to prepare ^{13}C-CNSI [73,130,132]. The quantification of CNSI in drainage lymph nodes was achieved by IRMS, indicating 0.011%–0.027% of the total injection amount migrated into drainage lymph nodes and the majority retained in the injection site. The quantitative information explained the high biosafety of CNSI, because only very a few of carbon NPs migrated in body and the rest would be dissected during oncological surgery. The persistent accumulation of CNSI in tumor inspired the drug development by intratumoral injection. The CNSI-Fe^{2+} complex was prepared by simply mixing CNSI and Fe^{2+}. ^{13}C-CNSI-Fe^{2+} mainly accumulated in tumor and the migration to other organs was not detected after 1 d [166]. The CNSI-Fe^{2+} complex showed meaningful antitumor activity by the arousal of extensive reactive oxygen species (ROS). After intravenous injection, CNSI-Fe^{2+} accumulated in liver and spleen, just as other carbon nanomaterials. The hepatic and splenic toxicity evaluations indi-

cated the low toxicity of CNSI-Fe^{2+} in mice. Currently, the preclinical studies of CNSI-Fe^{2+} have finished and CNSI-Fe^{2+} would hopefully be evaluated in clinical trials in near future.

Traditionally, deuterium, the stable isotope of hydrogen, and fluorine have been applied for drug molecular design and medicinal chemistry in past years [167–169], due to their unique physicochemical properties and utility in mechanistic, spectroscopic, and tracer studies. These elements were combined into the small molecular of the active pharmaceutical ingredient, which provided deeper insights into the kinetic isotope effect of labeled substance on the metabolic profile, distribution, and disposition of a drug. In future, the ^{2}H and ^{19}F labeled drug molecules might be loaded onto NPs for drug applications and the complex could be studied following the well-established protocols for small drug molecules.

6. Conclusion and perspectives

In summary, the advantages of skeleton stable isotope labeling include high accuracy, low detection limit, nonradioactive nature, high stability, and suitability in long-term tracing. The stable isotopes (^{13}C and metal isotopes) were incorporated/substituted directly into the skeleton carbon/metal atoms of these nanomaterials, while their stability, intrinsic nanostructures and chemical properties kept intact. Thus, the stable isotope labeling technique is ideal to quantify the *in vivo* behaviors of nanomaterials in complex biota and ecological environments. The quantitative information has largely benefited the biosafety evaluations of commercial nanomaterials and nanomedicine. In future, developments in analytical methods/technologies, with high spatial resolution, high sensitivity and multi-informative techniques or combined methods, and based on stable isotope techniques, are urgently required to support the fundamental studies on the uptake and transport pathways of NPs in the environment and biota system, and to obtain qualitative and quantitative information on the accumulation, location and speciation of NPs in environment and organism system. The quantifications and toxicity evaluations of different nanomaterials using similar protocols would benefit the understanding of the unique nano-bio-effects, such as the shape effect, size effect, and surface effect [3,21,54]. The metabolite analysis of stable isotope labeled nanomaterials is highly demanded [18,111,123,140]. We believe that the current knowledge will benefit the ongoing biomedical applications and environmental risk assessments of nanomaterials. However, it is still incomplete and not enough, while a lot of questions remain open. Compared to the stable isotope systems applied in traditional fields which have evolved over more than half a century, the research on carbon/metal stable isotope signatures for the application of biomedical effects and biosafety with labeled nanomaterials is still in its immature stage. More relevant investigations should go forward to light on insight for sustainable development of nanotechnology in the application of drug discovery and environmental control.

Declaration of competing interest

The authors declare that they have no known competing financial interests or personal relationships that could have appeared to influence the work reported in this paper.

Acknowledgments

We acknowledge financial support from the National Key Research and Development Program of China (No. 2021YFA1200904), the Beijing Natural Science Foundation (No. 2202065), the Fundamental Research Funds for the Central Universities, Southwest Minzu University (No. 2021PTJS36), and Major instrument project of National Natural Science Foundation of China (No. 22027810).

Supplementary materials

Supplementary material associated with this article can be found, in the online version, at doi:10.1016/j.cclet.2022.03.057.

References

[1] W.I. Hagens, A.G. Oomen, W.H. De Jong, F.R. Cassee, A.J.A.M. Sips, Regul. Toxicol. Pharm. 49 (2007) 217–229.
[2] S.J. Klaine, P.J.J. Alvarez, G.E. Batley, et al., Environ. Toxicol. Chem. 27 (2008) 1825–1851.
[3] A.E. Nel, L. Madler, D. Velegol, et al., Nat. Mater. 8 (2009) 543–557.
[4] R.F. Service, Science 300 (2003) 243.
[5] G. Oberdörster, E. Oberdörster, J. Oberdörster, Environ. Health Perspect. 113 (2005) 823–839.
[6] A.D. Maynard, R.J. Aitken, T. Butz, et al., Nature 444 (2006) 267–269.
[7] E. Oberdörster, S. Zhu, T.M. Blickley, P. Mcclellan-Green, M.L. Haasch, Carbon 44 (2006) 1112–1120.
[8] A. Nel, T. Xia, L. Madler, N. Li, Science 311 (2006) 622–627.
[9] J.M. Balbus, A.D. Maynard, V.L. Colvin, et al., Environ. Health Perspect. 115 (2007) 1654–1659.
[10] A. Nel, Y. Zhao, L. Mädler, Acc. Chem. Res. 46 (2013) 605–606.
[11] P. Westerhoff, B. Nowack, Acc. Chem. Res. 46 (2012) 844–853.
[12] J. Riego-Sintes, Nature 482 (2012) 35.
[13] P. Miralles, T.L. Church, A.T. Harris, Environ. Sci. Technol. 46 (2012) 9224–9239.
[14] A. Kahru, A. Ivask, Acc. Chem. Res. 46 (2012) 823–833.
[15] P.A. Holden, R.M. Nisbet, H.S. Lenihan, et al., Acc. Chem. Res. 46 (2013) 813–822.
[16] Y. Zhao, G. Xing, Z. Chai, Nat. Nanotechnol. 3 (2008) 191–192.
[17] X. He, Z. Zhang, J. Liu, et al., Nat. Nanotechnol. 6 (2011) 755.
[18] C.Y. Chen, Y.F. Li, Y. Qu, Z.F. Chai, Y.L. Zhao, Chem. Soc. Rev. 42 (2013) 8266–8303.
[19] Y. Liu, Y.L. Zhao, B.Y. Sun, C.Y. Chen, Acc. Chem. Res. 46 (2013) 702–713.
[20] M. Zhu, G. Nie, H. Meng, et al., Acc. Chem. Res. 46 (2013) 622–631.
[21] L. Wang, L. Yan, J. Liu, C. Chen, Y. Zhao, Anal. Chem. 90 (2018) 589–614.
[22] J. Wang, Z. Hu, J. Xu, Y. Zhao, NPG Asia Mater. 6 (2014) e84.
[23] Y.L. Zhao, X.L. Chang, Y.L. Zhao, Z. Zhang, W. Feng, Stable isotopic tracing of nanomaterials *in vivo*, Toxicology of Nanomaterials, John Wiley & Sons, 2016, pp. 43–67.
[24] X. He, Y. Ma, M. Li, et al., Small 9 (2013) 1482–1491.
[25] H. Wang, S.T. Yang, A. Cao, Y. Liu, Acc. Chem. Res. 46 (2013) 750–760.
[26] X.L. Chang, S.T. Yang, Y.L. Zhao, Sci. Sin. Chem. 46 (2016) 173–187.
[27] H.C. Wu, X.L. Chang, L. Liu, F. Zhao, Y.L. Zhao, J. Mater. Chem. 20 (2010) 1036–1052.
[28] S. Han, Y. Liu, X. Nie, et al., Small 8 (2012) 1596–1606.
[29] W. Li, C. Chen, C. Ye, et al., Nanotechnology 19 (2008) 145102.
[30] M. Cao, R. Cai, L. Zhao, et al., Nat. Nanotechnol. 16 (2021) 708–716.
[31] H.S. Leong, K.S. Butler, C.J. Brinker, et al., Nat. Nanotechnol. 14 (2019) 629–635.
[32] Y.L. Wang, R. Cai, C.Y. Chen, Acc. Chem. Res. 52 (2019) 1507–1518.
[33] E. Oberdörster, Environ. Health Perspect. 112 (2004) 1058–1062.
[34] F. Gottschalk, T. Sonderer, R.W. Scholz, B. Nowack, Environ. Sci. Technol. 43 (2009) 9216–9222.
[35] N.A. Lewinski, H. Zhu, H.J. Jo, et al., Environ. Sci. Technol. 44 (2010) 1841–1846.
[36] B. Wu, Y. Wang, Y.H. Lee, et al., Environ. Sci. Technol. 44 (2010) 1484–1489.
[37] B.D. Johnston, T.M. Scown, J. Moger, et al., Environ. Sci. Technol. 44 (2010) 1144–1151.
[38] R.F. Domingos, D.F. Simon, C. Hauser, K.J. Wilkinson, Environ. Sci. Technol. 45 (2011) 7664–7669.
[39] E.J. Petersen, L. Zhang, N.T. Mattison, et al., Environ. Sci. Technol. 45 (2011) 9837–9856.
[40] F. Larner, Y. Dogra, A. Dybowska, et al., Environ. Sci. Technol. 46 (2012) 12137–12145.
[41] P.N. Wiecinski, K.M. Metz, T.C. King Heiden, et al., Environ. Sci. Technol. 47 (2013) 9132–9139.
[42] X.L. Chang, L. Ruan, S.T. Yang, et al., Environ. Sci. Nano 1 (2014) 64–70.
[43] C. Wang, X.L. Chang, Q. Shi, X. Zhang, Environ. Sci. Technol. 52 (2018) 12133–12141.
[44] C. Wang, H. Zhang, L. Ruan, et al., Environ. Sci. Nano 3 (2016) 799–805.
[45] M. Du, H. Zhang, J. Li, et al., Environ. Sci. Technol. 50 (2016) 10421–10427.
[46] Q. Shi, C. Wang, H. Zhang, et al., Environ. Sci. Nano 7 (2020) 1240–1251.
[47] S.T. Yang, K.A.S. Fernando, J.H. Liu, J. Wang, Y.P. Sun, Small 4 (2008) 940–944.
[48] S.T. Yang, X. Wang, G. Jia, et al., Toxicol. Lett. 181 (2008) 182–189.
[49] S.T. Yang, W. Guo, Y. Lin, et al., J. Phys. Chem. C 111 (2007) 17761–17764.
[50] P. Wang, X. Nie, Y. Wang, et al., Small 9 (2013) 3799–3811.
[51] J. Saleem, L. Wang, C. Chen, Adv. Healthcare Mater. 7 (2018) 1800525.
[52] X. Lu, Y. Zhu, R. Bai, et al., Nat. Nanotechnol. 14 (2019) 719–727.
[53] A.R. Deline, J.A. Nason, Environ. Sci. Nano 6 (2019) 1043–1066.
[54] E.J. Petersen, M. Mortimer, R.M. Burgess, et al., Environ. Sci. Nano 6 (2019) 1619–1656.
[55] Q. Abbas, B. Yousaf, H. Ullah, et al., Crit. Rev. Environ. Sci. Technol. 50 (2020) 2523–2581.

[56] P. Zhang, S. Misra, Z. Guo, M. Rehkämper, E. Valsami-Jones, Nat. Protoc. 14 (2019) 2878–2899.
[57] T.C. Chao, G. Song, N. Hansmeier, et al., Anal. Chem. 83 (2011) 1777–1783.
[58] C.W. Isaacson, C.Y. Usenko, R.L. Tanguay, J.A. Field, Anal. Chem. 79 (2007) 9091–9097.
[59] A. Kolkman, E. Emke, P.S. Bäuerlein, et al., Anal. Chem. 85 (2013) 5867–5874.
[60] L.E. Murr, K.F. Soto, E.V. Esquivel, et al., JOM 56 (2004) 28–31.
[61] A. Astefanei, O. Núñez, M.T. Galceran, Anal. Chim. Acta 882 (2015) 1–21.
[62] C.W. Isaacson, M. Kleber, J.A. Field, Environ. Sci. Technol. 43 (2009) 6463–6474.
[63] K. Scida, P.W. Stege, G. Haby, G.A. Messina, C.D. García, Anal. Chim. Acta 691 (2011) 6–17.
[64] R. Avanasi, W.A. Jackson, B. Sherwin, J.F. Mudge, T.A. Anderson, Environ. Sci. Technol. 48 (2014) 2792–2797.
[65] X. Huang, H. Liu, D. Lu, et al., Chem. Soc. Rev. 50 (2021) 5243–5280.
[66] H.F. Wang, J. Wang, X.Y. Deng, et al., J. Nanosci. Nanotechnol. 4 (2004) 1019–1024.
[67] S.T. Yang, X. Wang, H.F. Wang, et al., J. Phys. Chem. C 113 (2009) 18110–18114.
[68] S.T. Yang, L. Cao, P.G.J. Luo, et al., J. Am. Chem. Soc. 131 (2009) 11308–11309.
[69] Y.P. Sun, B. Zhou, Y. Lin, et al., J. Am. Chem. Soc. 128 (2006) 7756–7757.
[70] G. Oberdörster, J.N. Finkelstein, C. Johnston, et al., Res. Rep. Health Eff. Inst. (2000) 75–86.
[71] G. Oberdörster, Z. Sharp, V. Atudorei, et al., J. Toxicol. Environ. Health A 65 (2002) 1531–1543.
[72] G. Oberdörster, Z. Sharp, V. Atudorei, et al., Inhal. Toxicol. 16 (2004) 437–445.
[73] P. Xie, Q. Xin, S.T. Yang, et al., Int. J. Nanomed. 12 (2017) 4891–4899.
[74] J.H. Liu, S.T. Yang, X. Wang, et al., ACS Appl. Mater. Interfaces 6 (2014) 14672–14678.
[75] C. Wang, Y. Bai, H. Li, et al., Part. Fibre Toxicol. 13 (2016) 14.
[76] K.R. Guo, M. Adeel, F. Hu, et al., J. Nanosci. Nanotechnol. 21 (2021) 3197–3202.
[77] Q. Shi, H. Zhang, C. Wang, et al., Ecotoxicol. Environ. Saf. 191 (2020) 110173.
[78] L. Chen, C. Wang, S. Yang, et al., Environ. Sci. Nano 4 (2019) 1077–1088.
[79] L. Chen, C. Wang, H. Li, et al., Environ. Sci. Technol. 51 (2017) 10146–10153.
[80] M. Guo, L. Zhao, J. Liu, et al., Nano Lett. 21 (2021) 6005–6013.
[81] Y. Xu, Y.H. Li, Y. Wang, et al., Analyst 139 (2014) 5134–5139.
[82] Q. Shi, C. Fang, C. Yan, et al., Ecotoxicol. Environ. Saf. 232 (2022) 113226.
[83] T.D. Berry, T.R. Filley, A.P. Clavijo, M. Bischoff Gray, R. Turco, Environ. Sci. Technol. 51 (2017) 1387–1394.
[84] T.D. Berry, A.P. Clavijo, Y. Zhao, et al., Environ. Pollut. 211 (2016) 338–345.
[85] K.M. Schreiner, T.R. Filley, R.A. Blanchette, et al., Environ. Sci. Technol. 43 (2009) 3162–3168.
[86] S.R. Chae, D.E. Hunt, K. Ikuma, et al., Water Res. 65 (2014) 282–289.
[87] S.K. Hanna, R.J. Miller, H.S. Lenihan, J. Hazard. Mater. 279 (2014) 32–37.
[88] J. Gigault, V.A. Hackley, Anal. Chim. Acta 763 (2013) 57–66.
[89] M.N. Croteau, A.D. Dybowska, S.N. Luoma, S.K. Misra, E. Valsami-Jones, Environ. Chem. 11 (2014) 247–256.
[90] A. Laycock, B. Stolpe, I. Römer, et al., Environ. Sci. Nano 1 (2014) 271–283.
[91] S. Yu, Y. Yin, X. Zhou, L. Dong, J. Liu, Environ. Sci. Nano 3 (2016) 883–893.
[92] J. Nath, I. Dror, P. Landa, et al., Environ. Pollut. 242 (2018) 1827–1837.
[93] Q. Yang, W. Shan, L. Hu, et al., Environ. Sci. Technol. 53 (2019) 625–633.
[94] Z. Shao, P. Guagliardo, H. Jiang, W.X. Wang, Environ. Sci. Technol. 55 (2021) 433–446.
[95] B. Gulson, M. Mccall, M. Korsch, et al., Toxicol. Sci. 118 (2010) 140–149.
[96] B. Gulson, H. Wong, M. Korsch, et al., Sci. Total Environ. 420 (2012) 313–318.
[97] F. Larner, B. Gulson, M. Mccall, Y. Oytam, M. Rehkämper, J. Anal. At. Spectrom. 29 (2014) 471–477.
[98] P.L. Lee, B.C. Chen, G. Gollavelli, et al., J. Hazard. Mater. 277 (2014) 3–12.
[99] M.J. Osmond-Mcleod, Y. Oytam, J.K. Kirby, et al., Nanotoxicology 8 (Suppl. 1) (2014) 72–84.
[100] A.D. Dybowska, M.N. Croteau, S.K. Misra, et al., Environ. Pollut. 159 (2011) 266–273.
[101] P.E. Buffet, C. Amiard-Triquet, A. Dybowska, et al., Ecotoxicol. Environ. Saf. 84 (2012) 191–198.
[102] A. Laycock, B. Coles, K. Kreissig, M. Rehkämper, J. Anal. At. Spectrom. 31 (2016) 297–302.
[103] A. Praetorius, A. Gundlach-Graham, E. Goldberg, et al., Environ. Sci. Nano 4 (2017) 307–314.
[104] P. Bonnand, C. Israel, M. Boyet, R. Doucelance, D. Auclair, J. Anal. At. Spectrom. 34 (2019) 504–516.
[105] A. Bourgeault, C. Cousin, V. Geertsen, et al., Environ. Sci. Technol. 49 (2015) 2451–2459.
[106] R.M. Handler, B.L. Beard, C.M. Johnson, M.M. Scherer, Environ. Sci. Technol. 43 (2009) 1102–1107.
[107] B. Meermann, K. Wichmann, F. Lauer, F. Vanhaecke, T.A. Ternes, J. Anal. At. Spectrom. 31 (2016) 890–901.
[108] S.K. Misra, A. Dybowska, D. Berhanu, et al., Environ. Sci. Technol. 46 (2012) 1216–1222.
[109] M.N. Croteau, S.K. Misra, S.N. Luoma, E. Valsami-Jones, Environ. Sci. Technol. 48 (2014) 10929–10937.
[110] K. Tiede, A.B.A. Boxall, S.P. Tear, et al., Food Addit. Contam. Part A 25 (2008) 795–821.
[111] B. Gulson, H. Wong, Environ. Health Perspect. 114 (2006) 1486–1488.
[112] R. Bullard-Dillard, K.E. Creek, W.A. Scrivens, J.M. Tour, Bioorg. Chem. 24 (1996) 376–385.
[113] J.Y. Xu, Q.N. Li, J.G. Li, et al., Carbon 45 (2007) 1865–1870.
[114] S. Yamago, H. Tokuyama, E. Nakamura, et al., Chem. Biol. 2 (1995) 385–389.
[115] S.C.J. Sumner, T.R. Fennell, R.W. Snyder, G.F. Taylor, A.H. Lewin, J. Appl. Toxicol. 30 (2010) 354–360.
[116] H. Song, S. Luo, H. Wei, et al., J. Radioanal. Nucl. Chem. 285 (2010) 635–639.
[117] Y.G. Li, X. Huang, R.L. Liu, et al., J. Radioanal. Nucl. Chem. 265 (2005) 127–131.
[118] N. Nadežda, V.Đ. Sanja, J. Drina, et al., Nanotechnology 20 (2009) 385102.
[119] Q. Li, Y. Xiu, X. Zhang, et al., Nucl. Med. Biol. 29 (2002) 707–710.
[120] D.W. Cagle, S.J. Kennel, S. Mirzadeh, J.M. Alford, L.J. Wilson, Proc. Natl. Acad. Sci. U. S. A. 96 (1999) 5182–5187.
[121] X.Y. Deng, S.T. Yang, H.Y. Nie, H.F. Wang, Y.F. Liu, Nanotechnology 19 (2008) 075101.
[122] Y. Yuan, X. Wang, G. Jia, et al., Diam. Relat. Mater. 19 (2010) 291–299.
[123] S. Stürup, H.R. Hansen, B. Gammelgaard, Anal. Bioanal. Chem. 390 (2008) 541–554.
[124] J.G. Wiederhold, Environ. Sci. Technol. 49 (2015) 2606–2624.
[125] R. Liu, S. Zhang, C. Wei, et al., Acc. Chem. Res. 49 (2016) 775–783.
[126] D. Lu, T. Zhang, X. Yang, et al., J. Anal. At. Spectrom. 32 (2017) 1848–1861.
[127] Y. Yin, Z. Tan, L. Hu, et al., Chem. Rev. 117 (2017) 4462–4487.
[128] J. Lv, P. Christie, S. Zhang, Environ. Sci. Nano 6 (2019) 41–59.
[129] Z. Muccio, G.P. Jackson, Analyst 134 (2009) 213–222.
[130] C. Wang, L. Ruan, X.L. Chang, et al., RSC Adv. 5 (2015) 76949–76956.
[131] Z.Z. Wang, X.L. Chang, Z.H. Lu, et al., Chem. Sci. 5 (2014) 2940–2948.
[132] L.F. Ruan, X.L. Chang, B.Y. Sun, et al., Chin. Sci. Bull. 59 (2014) 905–912.
[133] F. Simon, C. Kramberger, R. Pfeiffer, et al., Phys. Rev. Lett. 95 (2005) 017401.
[134] A. Kitaygorodskiy, W. Wang, S.Y. Xie, et al., J. Am. Chem. Soc. 127 (2005) 7517–7520.
[135] L. Liu, S. Fan, J. Am. Chem. Soc. 123 (2001) 11502–11503.
[136] L.B. Casabianca, M.A. Shaibat, W.W. Cai, et al., J. Am. Chem. Soc. 132 (2010) 5672–5676.
[137] W. Gao, L.B. Alemany, L. Ci, P.M. Ajayan, Nat. Chem. 1 (2009) 403–408.
[138] W. Cai, R.D. Piner, F.J. Stadermann, et al., Science 321 (2008) 1815–1817.
[139] A.L. Blumenfeld, V.E. Muradyan, I.B. Shumilova, Z.N. Parnes, Y.N. Novikov, Mater. Sci. Forum 91-93 (1992) 613–617.
[140] A.E. Mutlib, Chem. Res. Toxicol. 21 (2008) 1672–1689.
[141] B. Faubert, A. Tasdogan, S.J. Morrison, T.P. Mathews, R.J. Deberardinis, Nat. Protoc. 16 (2021) 5123–5145.
[142] A. Rodionov, E. Lehndorff, C.C. Stremtan, et al., Anal. Chem. 91 (2019) 6225–6232.
[143] L.N. Zheng, L.X. Feng, J.W. Shi, et al., Anal. Chem. 92 (2020) 14339–14345.
[144] D.L. Plata, P.M. Gschwend, C.M. Reddy, Nanotechnology 19 (2008) 185706.
[145] L. Tian, X. Wang, L. Cao, M.J. Meziani, Y.P. Sun, J. Nanomater. 2010 (2010) 742167.
[146] P.J. Horoyski, M.L.W. Thewalt, T.R. Anthony, Phys. Rev. B 54 (1996) 920–929.
[147] P.W. Dunk, N.K. Kaiser, C.L. Hendrickson, et al., Nat. Commun. 3 (2012) 855.
[148] T.W. Ebbesen, J. Tabuchi, K. Tanigaki, Chem. Phys. Lett. 191 (1992) 336–338.
[149] Y. Bai, X. Wu, P. Ouyang, et al., Environ. Sci. Nano 8 (2021) 76–85.
[150] J. Jin, M. Guo, J. Liu, et al., ACS Appl. Mater. Interfaces 10 (2018) 8436–8442.
[151] X.D. Li, M.Y. Guo, C.Y. Chen, Chem. Res. Chin. Univ. 37 (2021) 1176–1194.
[152] W.D. Allen, R.H. Dawton, M.L. Smith, P.C. Thonemann, Nature 175 (1955) 101–103.
[153] S.J. Yu, Y.J. Lai, L.J. Dong, J.F. Liu, Environ. Sci. Technol. 53 (2019) 10218–10226.
[154] T. Junk, M. Rehkämper, A. Laycock, J. Anal. At. Spectrom. 34 (2019) 1173–1183.
[155] F. Larner, L.N. Woodley, S. Shousha, et al., Metallomics 7 (2015) 112–117.
[156] F.R. Khan, A. Laycock, A. Dybowska, et al., Environ. Sci. Technol. 47 (2013) 8532–8539.
[157] A. Laycock, M. Diez-Ortiz, F. Larner, et al., Environ. Sci. Technol. 50 (2016) 412–419.
[158] A. Laycock, A. Romero-Freire, J. Najorka, et al., Environ. Sci. Technol. 51 (2017) 12756–12763.
[159] C. Caldelas, F. Poitrasson, J. Viers, J.L. Araus, Environ. Sci. Nano 7 (2020) 1927–1941.
[160] J. Eagles, S.J. Fairweather-Tait, R. Self, Anal. Chem. 57 (1985) 469–471.
[161] J. He, S. Li, W. Shao, et al., J. Surg. Oncol. 102 (2010) 676–682.
[162] J. Yan, F. Xue, H. Chen, et al., Surg. Endosc. 28 (2014) 3315–3321.
[163] Q. Yang, X.D. Wang, J. Chen, et al., Tumor Biol. 33 (2012) 2341–2348.
[164] P. Xie, X. Tang, L. Li, et al., J. Nanosci. Nanotechnol. 16 (2016) 6910–6918.
[165] J. Gu, J. Wang, X. Nie, W. Wang, J. Shang, Int. J. Clin. Exp. Med. 8 (2015) 9640–9648.
[166] P. Xie, S.T. Yang, Y. Huang, et al., ACS Appl. Mater. Interfaces 12 (2020) 29094–29102.
[167] T. Pirali, M. Serafini, S. Cargnin, A.A. Genazzani, J. Med. Chem. 62 (2019) 5276–5297.
[168] T.G. Gant, J. Med. Chem. 57 (2014) 3595–3611.
[169] B.M. Johnson, Y.Z. Shu, X. Zhuo, N.A. Meanwell, J. Med. Chem. 63 (2020) 6315–6386.